ACS APPLIED MATERIALS & INTERFACES

Letter

www.acsami.org

Solution-Processed Hybrid Cathode Interlayer for Inverted Organic Solar Cells

Yulei Wu,[†,‡] Wenjun Zhang,[†] Xiaodong Li,[†] Chao Min,[†] Tonggang Jiu,[†] Yuejin Zhu,[‡] Ning Dai,*[,†,§] and Junfeng Fang*[,†]

[†]Ningbo Institute of Materials Technology and Engineering, Chinese Academy of Sciences, Ningbo 315201, China

[‡]Faculty of Physics, Ningbo University, Ningbo 315211, China

[§]National Laboratory for infrared physics, Shanghai Institute of Technical Physics, Chinese Academy of Sciences, Shanghai 200083, China

Supporting Information

ABSTRACT: A novel hybrid material CdS/2,9-Dimethyl-4,7-diphenyl-1,10-phenanthroline (CdS·BCP) was prepared from the decomposition of its organic soluble precursor complex $Cd(S_2COEt)_2$·(BCP) by low-temperature treatment. CdS·BCP, which integrated the favorable properties of solvent durability, and high electron mobility of CdS as well as the good hole blocking property of BCP, was designed and developed as the interface modification material to improve electron collection in bulk heterojunction organic solar cells (OSCs). The inverted OSCs with CdS·BCP as buffer layer on ITO showed improved efficiency compared with the pure CdS or BCP. Devices with CdS·BCP as interlayer exhibited excellent stability, only 14.19% decay of power conversion efficiencies (PCEs) was observed (from 7.47% to 6.41%) after stored in glovebox for 3264 h (136 days). Our results demonstrate promising potentials of hybrid materials as the interface modification layers in OSCs, and provide new insights for the development of new interface modification materials in the future.

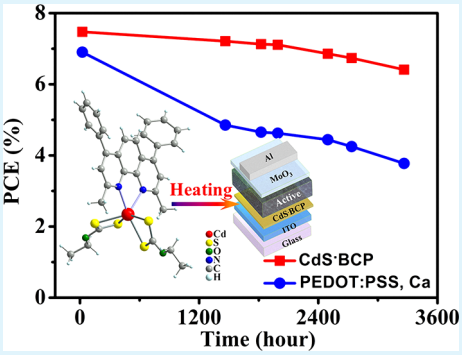

KEYWORDS: *OSCs, interface, hybrid, inverted, CdS, BCP*

1. INTRODUCTION

Organic solar cells (OSCs), as potential renewable energy sources, have attracted great attention because of their advantages of flexible mechanical property, lightweight, low cost, and ease of large area fabrication through roll-to-roll printing.[1−3] For the typical bulk heterojunction (BHJ) OSCs, an active layer composed of polymer light absorption donor and fullerene derivatives acceptor, is sandwiched between the anode and cathode.[3,4] The synthesis of light absorption donor materials and corresponding morphology control of the active layer has become a hot research topic, with many efforts dedicated to this field and power conversion efficiency (PCE) exceeding 9%.[5−9] In addition, another important research focus is the interfacial modification between the active layer and electrodes since interface properties directly affect the charge carrier collection, which is the crucial factor to realize high performance.[10−13] For conventional OSCs, the poly(3,4-ethylenedioxythiophene):poly(styrenesulfonate) (PEDOT:PSS) is spin-coated onto the indium tin oxide (ITO) as the buffer layer to improve the work function and morphology of the anode,[14] and low work function metals (like Ca and Ba) are used as the cathode. However, both PEDOT:PSS and low-work-function metals are important degradation factors of the devices because of their erosive or air-sensitive properties.[15]

To circumvent these problems, novel interface modification materials and inverted OSCs have been extensively investigated and shown promising device performance.[16,17] Metal oxides alternative to PEDOT:PSS are developed, such as molybdenum trioxide MoO_3,[18,19] tungsten trioxide WO_3,[20] nickel oxide NiO_x,[21] and vanadium pentoxide V_2O_5.[18] Inverted OSCs by using modified ITO as the cathode to collect the electrons were also widely studied. For inverted OSCs, the n-type interface buffer layer on top of ITO is the key issue for the device performance. The n-type buffer layer reported so far can be divided into two categories. One is based on organic materials.[22,23] The typical organic cathode buffer material is the well-known PFN, and recent inverted device efficiency based on PFN have reached 9.2%.[3] In addition to PFN, organic polar or charge materials are also electrostatically self-assembled onto the ITO or ITO/Metal oxide electrode to improve the device efficiency.[24−26] The other category is based on inorganic materials. Compared to organic materials, inorganic materials have better chemical stability and insolubility in organic solvents. This allows solution-processable multilayer device fabrication without any etching of buffer layer. Environmentally

Received: September 18, 2013
Accepted: October 18, 2013
Published: October 18, 2013

stable and highly transparent metal carbonate/oxides, such as Cs_2CO_3,[27] ZnO,[28,29] TiO_x,[30,31] SnO_x,[32] etc. have been demonstrated by several groups. However, formation of inorganic buffer layer usually requires high temperature (>200 °C). To be compatible with flexible substrates and low-cost, large area fabrication of the OSCs, much effort has been focused on solution-processing technology with low temperature treatment such as sol–gel methods, where organic or inorganic precursors decompose at low temperatures.[18−21,27−32]

In spite of these intensive research efforts on interlayer materials, it is interesting to note that the application of hybrid buffer layer materials in OSCS is potentially promising but currently lacking. Hybrid materials, a blend of organic and inorganic semiconductors, combine the advantages of organic and inorganic materials, have been intensively investigated in hybrid OSCs.[33] In this article, we reported CdS·2,9-Dimethyl-4,7-diphenyl-1,10-phenanthroline (CdS·BCP) hybrid cathode buffer materials for the inverted polymer solar cells. The hybrid film was fabricated by a low temperature in situ growth method from a single molecule solution. PCEs of the inverted devices based on CdS·BCP as the interlayer on ITO show impressive improvement and reach 7.47%. Compared with devices based on pure CdS (4.8%) or BCP (6.6%) as the interlayer, the efficiency improves by 56 and 13%, respectively. Our work indicates that the organic/inorganic hybrid materials are a promising candidate for cathode interlayer for OSCs.

2. RESULTS AND DISCUSSION

2,9-Dimethyl-4,7-diphenyl-1,10-phenanthroline (BCP or bathocuproine) is chosen as the organic material in the hybrid interlayer because of its excellent electron transporting and hole blocking properties, as demonstrated by numerous reports in organic light emitting diodes (OLEDs) and conventional structure OSCs.[34,35] As an excellent n-type semiconductor, CdS, which is widely used as buffer layer in inorganic solar cells like CZGS or CIGS,[36] is employed as the inorganic semiconductors in the hybrid interlayer. CdS nano materials, such as nanoparticles,[37] nanorods,[38] etc. are also widely used as the acceptor material in the hybrid bulk heterojunction solar cells.[33] The drawback of these nano materials for the OSC application is that ligand exchange is required to facilitate the charge transport, and thus the charge transfer between the donor and acceptor is hindered. Recently, Haque and co-workers reported the application of in situ growth of CdS in polymer/CdS hybrid bulk heterojunction solar cells through low-temperature decomposition of chelate precursor cadmium ethylxanthate.[39−41] Functional BCP was used as a ligand to chelate with cadmium xanthate to obtain a solution-processable precursor $Cd(S_2COEt)_2$·(BCP). The precursor $Cd(S_2COEt)_2$·(BCP) was synthesized according to the method as reported in ref 39 and purified by recrystallization from chloroform twice (Figure 1a). The light yellow crystal $Cd(S_2COEt)_2$·(BCP) can be dissolved in various solvents such as acetone, chloroform, chlorobenzene, etc. After low temperature treatment (~150–170 °C), the ethylxanthate part broke down to low boiling point product and formed CdS,[40] but BCP chelated with CdS and resulted in CdS·BCP hybrid materials. The component of BCP in $Cd(S_2COEt)_2$·(BCP) made it easy for solution-processing and improved the film morphology, whereas the component of CdS made the CdS·BCP film insoluble in organic solvents, which allows the fabrication of multilayer devices. Furthermore, the excellent electrical properties of CdS

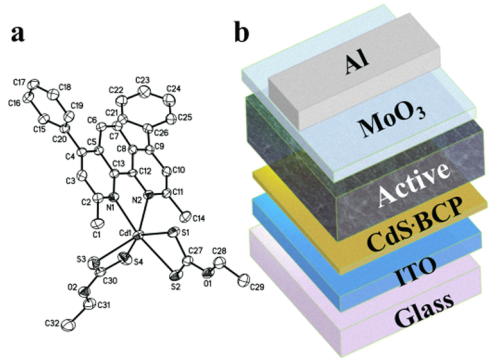

Figure 1. (a) Structure of $Cd(S_2COEt)_2$·(BCP) (without H atoms). (b) Structure of the inverted OSCs with CdS·BCP as electron transport layer.

were integrated in the CdS·BCP as well. To fabricate OSCs, we spin-coated $Cd(S_2COEt)_2$·(BCP) onto ITO substrate through its acetone solution and decomposed to CdS·BCP at 175 °C for 20 min, poly[[4,8-bis[(2-ethylhexyl)oxy]benzo[1,2-b:4,5-b′]-dithiophene-2,6-diyl][3-fluoro-2-[(2-ethylhexyl)carbonyl]thieno[3,4-b]thiophenediyl]] (PTB7) and [6,6]-phenyl-C71-butyric acid methyl ester ($PC_{71}BM$) blend was used as BHJ active layer,[5,42] MoO_3/Al was evaporated as the positive electrode (Figure 1b).

Figure 2 shows the current density versus voltage curves of CdS·BCP (30 nm) based devices under the illumination of

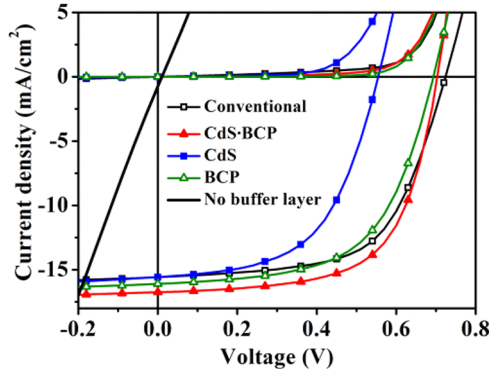

Figure 2. Current density–voltage curves of inverted devices ITO/buffer layer/PTB7:$PC_{71}BM$/MoO_3/Al using CdS·BCP, CdS, and BCP as buffer layer respectively, the conventional device ITO/PEDOT:PSS/PTB7:$PC_{71}BM$/Ca/Al.

AM1.5, 100 mW/cm^2. Inverted devices without any buffer layer (bare ITO) and the conventional devices with ITO/PEDOT:PSS (40 nm) and Ca (20 nm)/Al as the electrode were fabricated by using the same PTB7:$PC_{71}BM$ solution for comparison. The detailed results are summarized in Table 1. Devices without any buffer layer (bare ITO) show almost no photovoltaic behavior. After modification of ITO with CdS·BCP, the devices show a high PCE of 7.47%, with the open circuit voltage (V_{oc}) of 0.70 V and short current density (J_{sc}) of 16.74 mA/cm^2. The fill factor (FF) is as high as 63.49% and the average PCE of 48 devices is 7.3%, while devices with the controlled conventional structures only show an average PCE of 6.8% (best PCE of 6.9%). The 7.4% improvements in PCEs compared with the conventional device were mainly ascribed to the increase of J_{sc} from 15.55 mA/cm^2 to 16.74 mA/cm^2 (increased by 7.7%). To better understand the interfacial

dx.doi.org/10.1021/am404053e | ACS Appl. Mater. Interfaces 2013, 5, 10428−10432

Table 1. Performances of OSCs with Different Buffer Layers and Device Structures Are Shown Below[a]

interlayer	V_{oc} (V)	J_{sc} (mA/cm^{-2})	FF (%)	PCE (%)	avg[b] (%)
PEDOT	0.724	15.55	61.31	6.90	6.81
CdS·BCP	0.703	16.74	63.49	7.47	7.31
CdS	0.554	15.58	55.27	4.77	4.46
BCP	0.694	16.09	58.82	6.57	6.44

[a]The PEDOT:PSS is used in conventional devices, and the others are used in inverted devices. Figure S2 shows the reproducibility of devices as listed below. [b]16 devices for PEDOT:PSS, 48 devices for CdS·BCP, 25 devices for the CdS, 21 devices for BCP.

modification function of CdS·BCP hybrid material, we also fabricated devices with pure CdS (25 nm) and BCP (40 nm) as the ITO modifiers. CdS was formed by treatment of its soluble precursor with pyridine as the ligand,[39] and BCP was spin-coated from its chloroform solution. Both CdS and BCP based devices (treated at 175 °C) show moderate PCEs (4.5 and 6.4%). CdS-based devices demonstrate high J_{sc} of 15.58 mA/cm^2. But the low V_{oc} of only 0.55 V seriously limited the PCEs (4.5%). The PCE of BCP-based devices without annealing treatment is only 2.84% with a V_{oc} of 0.44 V, a J_{sc} of 15.37 mA/cm^2, and an FF of 42.45%. But after treating at 175 °C the efficiency was improved significantly to a PCE of 6.57% and is close to the control conventional devices (6.90%). As far as we know, this is also the first report on the solution processsed BCP as the buffer layer for the high efficiency inverted OSC. The V_{oc} was improved to 0.69 V, which is much higher than CdS based devices (0.56 V) and comparable to the CdS·BCP hybrid devices. The improvements of V_{oc} are ascribed to the good hole blocking function of BCP and the alleviated recombination near the electrode.[35] J_{sc} and FF are, however, all lower than those of CdS·BCP hybrid devices, implying that the CdS part of CdS·BCP hybrid materials also plays an important role. CdS is a well-known n-type material and has good electron transport ability, which will improve the conduction properties of the hybrid material. As a result, the contact resistance and charge carrier recombination could also be decreased. The data summarized in Table S1 in the Supporting Information indicate that the series resistance of CdS·BCP is the lowest and the shunt resistance is the highest in these charge injection materials. The above results indicate that hybrid interlayer by integrating inorganic CdS and organic BCP together outperforms pure CdS or BCP significantly. The intensity of external quantum efficiency (EQE, Figure S1 in the Supporting Information) with different buffer layers are consistent with the corresponding J_{sc}. CdS and the controlled PEDOT:PSS based devices show lower overall EQE, EQE of CdS·BCP is comparable to that of BCP. CdS·BCP shows ~8.5% higher EQE than CdS at most wavelength range, which implies a more efficient carrier extraction function. The above-mentioned results indicate that hybrid modifier by integrating inorganic CdS and organic BCP together outperforms pure CdS or BCP obviously.

Thermogravimetric analysis (TGA) of precursor Cd(S$_2$COEt)$_2$·(BCP) was performed to understand the decomposition process (see Figure S3 in the Supporting Information). The precursor Cd(S$_2$COEt)$_2$·(BCP) has relative good thermal stability up to 130 °C and with ca. 5% weight loss at 146 °C. After 165 °C the TGA traces tend to flat with a weight loss of ~28%, which is well-consistent with the conversion from Cd(S$_2$COEt)$_2$·(BCP) (M_w = 715.02 g/mol) to CdS·BCP (M_w = 517.68 g/mol). The X-ray photoelectron spectroscopy (XPS) results of film treated at 175 °C for 20 min further confirmed this behavior (Figure 3). The atomic ratio of N and Cd

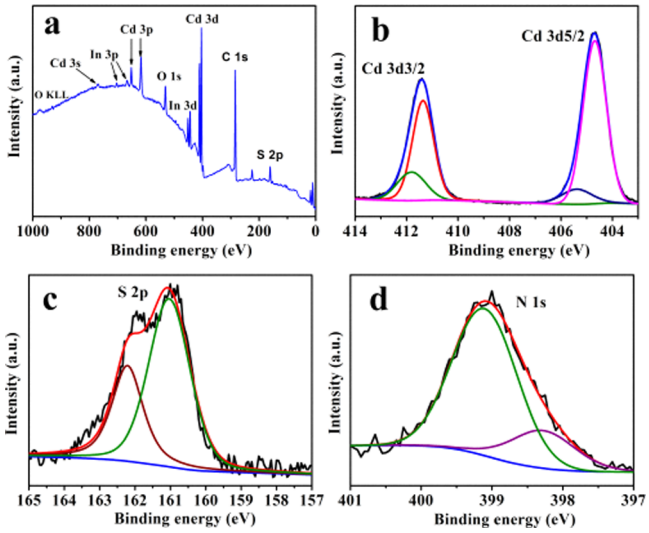

Figure 3. X-ray photoelectron spectroscopy (XPS) of CdS·BCP film on ITO substrate. (a) XPS survey spectrum, (b) Cd 3d, (c) S 2p, and (d) N 1s core level spectra.

calculated from the area of the N 1s and Cd 3d peaks is 1.96:1, which is in agreement with the ratio of CdS·BCP (2:1), and the ratio of S and Cd is about 1:1.2, which means that CdS is obtained. All XPS spectra were corrected based on the C 1s peak at 284.7 eV for determination of binding energy (BE) values of different elements. BE positions of Cd 3d3/2 and Cd 3d5/2 for the CdS·BCP film are at 411.4 and 404.7 eV, respectively, with a peak separation of 6.7 eV.[43] A peak shift to higher energy (411.8 and 405.2 eV, Figure 3b) is observed, which implies the change of electron cloud density of Cd in CdS. The doublet peak of S 2p with a 2:1 area ratio and a splitting of 1.2 eV identifies the formation of CdS.[44] The slight peak position shift of N 1s for CdS·BCP toward lower BE values (399.1 and 398.3 eV, respectively, Figure 3d), coupled with the peak shift of Cd 3d to higher energy, indicate the interaction between CdS and BCP through Cd−N bond. This means that, after 175 °C treatment, CdS and BCP still combine to each other through chemical bond.

Ultraviolet photon spectroscopy (UPS) was carried out to measure the work function of CdS·BCP film (see Figure S4 in the Supporting Information). The work-function of CdS·BCP was calculated to be 4.23 eV.[45] The electronic structures of materials used in the devices are all shown in Figure 4, the value of other materials in the devices are from literatures.[3,46] From the diagram, the work function of ITO is 4.7 eV, indicating a

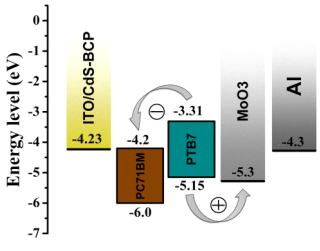

Figure 4. Energy levels of the materials involved in the inverted OSCs.

dx.doi.org/10.1021/am404053e | ACS Appl. Mater. Interfaces 2013, 5, 10428−10432

strong energy barrier for the electron transport. As a result, almost no photovoltaic behavior on devices used ITO as the cathode (Figure 2). After modified by CdS·BCP, the work function of ITO/CdS·BCP was effectively decreased to 4.23 eV which is comparable to the lowest unoccupied molecular orbital (LUMO) of $PC_{71}BM$ (4.2 eV). As a result, electrons on LUMO of $PC_{71}BM$ can be facilely transferred to ITO electrode through CdS·BCP and collected. Although absorption from the CdS·BCP may also potentially benefit the efficiency, low absorption of the hybrid materials (see Figure S5 in the Supporting Information) might indicate that improvements of the efficiency are mainly from the good carrier collection because of the proper work function and good transport ability. And the contribution from the optimized morphology of CdS·BCP film should also be important.

One of the important advantages of the inverted devices is good stability because of the absence of both active metal and PEDOT:PSS. Therefore, we also studied the stability of hybrid CdS·BCP based devices. To better understand the decay of the devices, we fabricated conventional devices with ITO/PEDOT:PSS and Ca/Al as the electrodes at the same time for the comparison (Figure 5). Both devices were fabricated

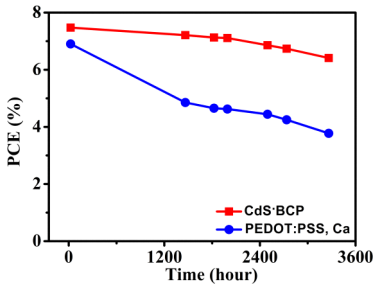

Figure 5. Stability of the PTB7-based inverted device using CdS·BCP as an interlayer. The stability of a conventional device using ITO/PEDOT:PSS and Ca/Al as the electrode is also recorded for comparison.

without any encapsulation and stored in the glovebox. After ~3264 h (~136 days), obvious decay of conventional device was observed, the efficiency decreased 45.4% (PCE from 6.9 to 3.8%). The decay is mainly due to the decrease in J_{sc} and FF. The erosion of ITO by PEDOT:PSS could be one of the main reasons. In addition, oxidation of Ca cannot be completely excluded even though the devices were stored in the inert environment. Anyhow, both effects lead to poorer interface properties and impede charge carrier collection, and hence the series resistance of the devices will also be increased, giving rise to the decrease of FF. In contrast, devices with hybrid CdS·BCP as the injection layer show impressive stability. No obvious decay in V_{oc} was observed (from 0.70 to 0.69 V). J_{sc} and FF decreased to 15.86 mA/cm^2 and 58.4% from 16.74 mA/cm^2 and 63.5%, respectively. Only 14.2% decay of PCEs was observed (from 7.47 to 6.4%) during the same time and at the same condition. Even with 14.2% decay, the PCE (6.4%) is still comparable to the initial PCEs of conventional device (6.9%). The impressive lifetime of the devices is ascribed to highly stable property of CdS·BCP and the inverted device structure. The lifetime experiments are still under way.

We also investigated the cathode modifying function of CdS·BCP for the different active materials (see Figure S6 and Table S2 in the Supporting Information). In addition to PTB7:$PC_{71}BM$ active layer, P3HT:$PC_{60}BM$, a well-known and widely studied system for OSCs,[47,48] has been tested as the bulk heterojunction layer. Compared to the conventional PEDOT:PSS and Ca-based devices (PCEs = 3.6%), the PCE of ITO/CdS·BCP-based converted devices shows an improvement of 11.6% so that it reaches 4.0%. Evidently, the interface modification of hybrid CdS·BCP does work for different active layers.

3. CONCLUSIONS

In summary, we fabricated CdS·BCP hybrid interlayers for OSCs using an in situ growth method. The device efficiency with hybrid interlayers shows significant improvement compared with the devices with pure CdS or pure BCP. In addition, we also demonstrated that the CdS·BCP hybrid interalyers are effective to both the highly efficient PTB7:$PC_{71}BM$ and the benchmark P3HT:$PC_{60}BM$ active layers, demonstrating the universal applicability of the approach. Devices with the hybrid interlayers also show good stability, with only 14.2% decay of PCEs observed for the devices stored in glovebox for 3264 h (45.4% for the conventional device at the same conditions). Our work suggests that inorganic semiconductor/organic semiconductor hybrid is a promising route to improve the performance of the organic electronic devices, and paves a way for a new class of interlayers in organic electronics.

■ ASSOCIATED CONTENT

Supporting Information

(1) Experimental details of precursors synthesis and devices fabrication; (2) EQE of devices that fabricated on different interlayers, reproducibility of devices, TGA, UPS, UV−vis spectra, the performance comparison between devices fabricated on CdS·BCP and PEDOT:PSS based on P3HT/PCBM system, and the crystal data of $Cd(S_2COEt)_2$·BCP. This material is available free of charge via the Internet at http://pubs.acs.org.

■ AUTHOR INFORMATION

Corresponding Authors

*E-mail: fangjf@nimte.ac.cn.

*E-mail: daining@nimte.ac.cn.

Notes

The authors declare no competing financial interest.

■ ACKNOWLEDGMENTS

The Project (51273208) supported by National Natural Science Foundation of China. The work was also supported by Hundred Talent Program of Chinese Academy of Sciences; the Starting Research Fund of Team Talent (Y10801RA01) in NIMTE; the Ningbo Natural Science Foundation of China (2012A610114); the National Key Basic Research Program of China (973 program, Grant 2012CB934300.

■ REFERENCES

(1) Gunes, S.; Neugebauer, H.; Sariciftci, N. S. *Chem. Rev.* **2007**, *107*, 1324−1338.

(2) Li, G.; Shrotriya, V.; Huang, J.; Yao, Y.; Moriarty, T.; Emery, K.; Yang, Y. *Nat. Mater.* **2005**, *4*, 864−868.

(3) He, Z.; Zhong, C.; Su, S.; Xu, M.; Wu, H.; Cao, Y. *Nat. Photonics* **2012**, *6*, 591−595.

(4) He, Z.; Zhong, C.; Huang, X.; Wong, W. Y.; Wu, H.; Chen, L.; Su, S.; Cao, Y. *Adv. Mater.* **2011**, *23*, 4636−4643.

(5) Liang, Y.; Xu, Z.; Xia, J.; Tsai, S. T.; Wu, Y.; Li, G.; Ray, C.; Yu, L. *Adv. Mater.* **2010**, *22*, 135−138.
(6) Huo, L. J.; Zhang, S. Q.; Guo, X.; Xu, F.; Li, Y. F.; Hou, J. H. *Angew. Chem., Int. Ed.* **2011**, *50*, 9697−9702.
(7) Lee, J. K.; Ma, W. L.; Brabec, C. J.; Yuen, J.; Moon, J. S.; Kim, J. Y.; Lee, K.; Bazan, G. C.; Heeger, A. J. *J. Am. Chem. Soc.* **2008**, *130*, 3619−3623.
(8) Li, W.; Furlan, A.; Hendriks, K. H.; Wienk, M. M.; Janssen, R. A. *J. Am. Chem. Soc.* **2013**, *135*, 5529−5532.
(9) You, J.; Dou, L.; Yoshimura, K.; Kato, T.; Ohya, K.; Moriarty, T.; Emery, K.; Chen, C. C.; Gao, J.; Li, G.; Yang, Y. *Nat. Commun.* **2013**, *4*, 1446−1455.
(10) Ma, H.; Yip, H. L.; Huang, F.; Jen, A. K. Y. *Adv. Funct. Mater.* **2010**, *20*, 1371−1388.
(11) Min, C.; Shi, C.; Zhang, W.; Jiu, T.; Chen, J.; Ma, D.; Fang, J. *Angew. Chem., Int. Ed.* **2013**, *52*, 3417−3420.
(12) Fang, J.; Wallikewitz, B. H.; Gao, F.; Tu, G.; Müller, C.; Pace, G.; Friend, R. H.; Huck, W. T. *J. Am. Chem. Soc.* **2010**, *133*, 683−685.
(13) Zhou, Y.; Hernandez, C. F.; Shim, J.; Meyer, J.; Giordano, A. J.; Li, H.; Winget, P.; Papadopoulos, T.; Cheun, H.; Kim, J. *Science* **2012**, *336*, 327−332.
(14) Zhang, F.; Johansson, M.; Andersson, M. R.; Hummelen, J. C.; Inganäs, O. *Adv. Mater.* **2002**, *14*, 662−665.
(15) Jørgensen, M.; Norrman, K.; Krebs, F. C. *Sol. Energy Mater. Sol. Cells* **2008**, *92*, 686−714.
(16) Chen, L. M.; Hong, Z.; Li, G.; Yang, Y. *Adv. Mater.* **2009**, *21*, 1434−1449.
(17) Li, G.; Chu, C. W.; Shrotriya, V.; Huang, J.; Yang, Y. *Appl. Phys. Lett.* **2006**, *88*, 253503.
(18) Shao, S.; Liu, J.; Bergqvist, J.; Shi, S.; Veit, C.; Würfel, U.; Xie, Z.; Zhang, F. *Adv. Energy Mater.* **2013**, *3*, 349−355.
(19) Fan, X.; Cui, C.; Fang, G.; Wang, J.; Li, S.; Cheng, F.; Long, H.; Li, Y. *Adv. Funct. Mater.* **2012**, *22*, 585−590.
(20) Tao, C.; Ruan, S.; Xie, G.; Kong, X.; Shen, L.; Meng, F.; Liu, C.; Zhang, X.; Dong, W.; Chen, W. *Appl. Phys. Lett.* **2009**, *94*, 043311−043313.
(21) Zhang, W.; Tan, Z. a.; Qian, D.; Xu, Q.; Li, L.; Li, S.; Wang, F.; Zheng, H.; Li, Y. *J. Appl. Polym. Sci.* **2012**, *128*, 684−690.
(22) Duan, C.; Zhang, K.; Guan, X.; Zhong, C.; Xie, H.; Huang, F.; Chen, J.; Peng, J.; Cao, Y. *Chem. Sci.* **2013**, *4*, 1298−1307.
(23) Henson, Z. B.; Zhang, Y.; Nguyen, T. Q.; Seo, J. H.; Bazan, G. C. *J. Am. Chem. Soc.* **2013**, *135*, 4163−4166.
(24) Motiei, L.; Yao, Y.; Choudhury, J.; Yan, H.; Marks, T. J.; Boom, M. E. v. d.; Facchetti, A. *J. Am. Chem. Soc.* **2010**, *132*, 12528−12530.
(25) Choi, H.; Park, J. S.; Jeong, E.; Kim, G. H.; Lee, B. R.; Kim, S. O.; Song, M. H.; Woo, H. Y.; Kim, J. Y. *Adv. Mater.* **2011**, *23*, 2759−2763.
(26) Ha, Y. E.; Jo, M. Y.; Park, J.; Kang, Y. C.; Yoo, S. I.; Kim, J. H. *J. Phys. Chem. C* **2013**, *117*, 2646−2652.
(27) Liao, H. H.; Chen, L. M.; Xu, Z.; Li, G.; Yang, Y. *Appl. Phys. Lett.* **2008**, *92*, 173303.
(28) Sun, Y.; Seo, J. H.; Takacs, C. J.; Seifter, J.; Heeger, A. J. *Adv. Mater.* **2011**, *23*, 1679−1683.
(29) Liu, J.; Shao, S.; Meng, B.; Fang, G.; Xie, Z.; Wang, L.; Li, X. *Appl. Phys. Lett.* **2012**, *100*, 213906.
(30) Tan, Z.; Yang, C.; Zhou, E.; Wang, X.; Li, Y. *Appl. Phys. Lett.* **2007**, *91*, 023503.
(31) Shao, S.; Zheng, K.; Pullerits, T.; Zhang, F. *ACS Appl. Mater. Interfaces* **2013**, *5*, 380−385.
(32) Trost, S.; Zilberberg, K.; Behrendt, A.; Riedl, T. *J. Mater. Chem.* **2012**, *22*, 16224−16229.
(33) Gao, F.; Ren, S.; Wang, J. *Energy Environ. Sci.* **2013**, *6*, 2020−2040.
(34) Adamovich, V. I.; Cordero, S. R.; Djurovich, P. I.; Tamayo, A.; Thompson, M. E.; D'Andrade, B. W.; Forrest, S. R. *Org. Electron.* **2003**, *4*, 77−87.
(35) Gommans, H.; Verreet, B.; Rand, B. P.; Muller, R.; Poortmans, J.; Heremans, P.; Genoe, J. *Adv. Funct. Mater.* **2008**, *18*, 3686−3691.
(36) Todorov, T. K.; Tang, J.; Bag, S.; Gunawan, O.; Gokmen, T.; Zhu, Y.; Mitzi, D. B. *Adv. Energy Mater.* **2013**, *3*, 34−38.
(37) Ren, S.; Chang, L. Y.; Lim, S. K.; Zhao, J.; Smith, M.; Zhao, N.; Bulović, V.; Bawendi, M.; Gradečak, S. *Nano Lett.* **2011**, *11*, 3998−4002.
(38) Kang, Y.; Kim, D. *Sol. Energy Mater. Sol. Cells* **2006**, *90*, 166−174.
(39) Leventis, H. C.; King, S. P.; Sudlow, A.; Hill, M. S.; Molloy, K. C.; Haque, S. A. *Nano lett.* **2010**, *10*, 1253−1258.
(40) Dowland, S.; Lutz, T.; Ward, A.; King, S. P.; Sudlow, A.; Hill, M. S.; Molloy, K. C.; Haque, S. A. *Adv. Mater.* **2011**, *23*, 2739−2744.
(41) Bansal, N.; O'Mahony, F. T.; Lutz, T.; Haque, S. A. *Sci. Rep.* **2013**, *3*, 1531.
(42) Liang, Y.; Yu, L. *Acc. Chem. Res.* **2010**, *43*, 1227−1236.
(43) Li, Y.; Liao, H.; Ding, Y.; Fan, Y.; Zhang, Y.; Qian, Y. *Inorg. Chem.* **1999**, *38*, 1382.
(44) Castner, D. G.; Hinds, K.; Grainger, D. W. *Langmuir* **1996**, *12*, 5083−5086.
(45) Michaelson, H. B. *J. Appl. Phys.* **1977**, *48*, 4729−4733.
(46) You, J.; Chen, C. C.; Dou, L.; Murase, S.; H. Duan, S.; Hawks, S.; Xu, T.; Son, H. J.; Yu, L.; Li, G.; Yang, Y. *Adv. Mater.* **2012**, *24*, 5267−5272.
(47) Kim, Y.; Cook, S.; Tuladhar, S. M.; Choulis, S. A.; Nelson, J.; Durrant, J. R.; Bradley, D. D. C.; Giles, M.; McCulloch, I.; Ha, C. S.; Ree, M. *Nat. Mater.* **2006**, *5*, 197−203.
(48) Gao, F.; Wang, J.; Blakesley, J. C.; Hwang, I.; Li, Z.; Greenham, N. C. *Adv. Energy Mater.* **2012**, *2*, 956−961.